2014

Thermoelectric performance of tellurium-reduced quaternary p-type lead-chalcogenide composites

Sima Aminorroaya Yamini
University of Wollongong, sima@uow.edu.au

Heng Wang
California Institute of Technology

Zachary M. Gibbs
California Institute of Technology

Yanzhong Pei
California Institute of Technology

David R. G Mitchell
University of Wollongong, dmitchel@uow.edu.au

See next page for additional authors

Publication Details

Yamini, S. Aminorroaya., Wang, H., Gibbs, Z. M., Pei, Y., Mitchell, D. R. G., Dou, S. Xue. & Snyder, G. Jeffrey. (2014). Thermoelectric performance of tellurium-reduced quaternary p-type lead-chalcogenide composites. Acta Materialia, 80 365-372.

Thermoelectric performance of tellurium-reduced quaternary p-type lead-chalcogenide composites

Abstract
A long-standing technological challenge to the widespread application of thermoelectric generators is obtaining high-performance thermoelectric materials from abundant elements. Intensive study on PbTe alloys has resulted in a high figure of merit for the single-phase ternary PbTe-PbSe system through band structure engineering, and the low thermal conductivity achieved due to nanostructuring leads to high thermoelectric performance for ternary PbTe-PbS compounds. Recently, the single-phase p-type quaternary PbTe-PbSe-PbS alloys have been shown to provide thermoelectric performance superior to the binary and ternary lead chalcogenides. This occurs via tuning of the band structure and from an extraordinary low thermal conductivity resulting from high-contrast atomic mass solute atoms. Here, we present the thermoelectric efficiency of nanostructured p-type quaternary PbTe-PbSe-PbS composites and compare the results with corresponding single-phase quaternary lead chalcogenide alloys. We demonstrate that the very low lattice thermal conductivity achieved is attributed to phonon scattering at high-contrast atomic mass solute atoms rather than from the contribution of secondary phases. This results in a thermoelectric efficiency of ~1.4 over a wide temperature range (650-850 K) in a p-type quaternary (PbTe)0.65(PbSe)0.1(PbS)0.25 composite that is lower than that of single-phase (PbTe)0.85(PbSe)0.1(PbS)0.05 alloy without secondary phases.

Keywords
lead, chalcogenide, composites, thermoelectric, tellurium, performance, reduced, quaternary, p, type

Publication Details
Yamini, S. Aminorroaya., Wang, H., Gibbs, Z. M., Pei, Y., Mitchell, D. R. G., Dou, S. Xue. & Snyder, G. Jeffrey. (2014). Thermoelectric performance of tellurium-reduced quaternary p-type lead-chalcogenide composites. Acta Materialia, 80 365-372.

Authors
Sima Aminorroaya Yamini, Heng Wang, Zachary M. Gibbs, Yanzhong Pei, David R. G Mitchell, S X. Dou, and G. Jeffrey Snyder

Thermoelectric performance of Tellurium-reduced quaternary *p*-type lead-chalcogenide composites

Sima Aminorroaya Yamini[1]*, Heng Wang[2] , Zachary M. Gibbs[3] , Yanzhong Pei[4] , David R.G.Mitchell[5] , Shi Xue Dou[1] and G Jeffrey Snyder[2,6]*

[1] Australian Institute for Innovative Materials (AIIM), Innovation Campus, University of Wollongong, NSW 2500, Australia.
[2] Materials Science, California Institute of Technology, Pasadena, CA 91125, USA.
[3] Division of Chemistry and Chemical Engineering, California Institute of Technology, Pasadena, CA 91125, USA.
[4] School of Materials Science and Engineering, Tongji University, 4800 Caoan Road, Shanghai 201804, China.
[5] Electron Microscopy Centre (EMC), Australian Institute for Innovative Materials (AIIM), Innovation Campus, University of Wollongong, NSW 2500, Australia.
[6] ITMO University, Saint Petersburg, Russia.

Abstract: A long-standing technological challenge to the widespread application of thermoelectric generators is obtaining high performance thermoelectric materials from abundant elements. The substantial studies on PbTe alloys result in a high figure of merit for the single phase ternary PbTe-PbSe system through band structure engineering, and the low thermal conductivity achieved due to nanostructuring leads to high thermoelectric performance for ternary PbTe-PbS compounds. Recently, the single phase *p*-type quaternary PbTe-PbSe-PbS alloys have been shown to provide thermoelectric performance superior to the binary and ternary lead chalcogenides. This occurs via tuning of the band structure and from an extraordinary low thermal conductivity resulting from high contrast atomic mass solute atoms.

Here, we present the thermoelectric efficiency of nanostructured *p*-type quaternary PbTe-PbSe-PbS composites and compare the results with corresponding single phase quaternary lead chalcogenide alloys. We demonstrate that the very low achieved lattice thermal conductivity is attributed to phonon scattering at high contrast atomic mass solute atoms rather than from the contribution of secondary phases. This results in a thermoelectric efficiency of ~ 1.4 over a wide temperature range (650 - 850 K) in a *p*-type quaternary $(PbTe)_{0.65}(PbSe)_{0.1}(PbS)_{0.25}$ composite that is lower than that of single phase $(PbTe)_{0.85}(PbSe)_{0.1}(PbS)_{0.05}$ alloy without secondary phases.

Keywords: Pb-chalcogenide; thermoelectric materials; cost-effective; composite.

1. Introduction

The world's demand for energy, as well as concerns about global warming, have inspired intensive research to develop clean and sustainable energy sources. Thermoelectric devices that convert heat to electricity are considered promising candidates for waste heat recovery [1], and the search continues to provide high performance thermoelectric materials from abundant earth elements. A large number of recent studies [2-8] have focused on the mid-range temperature (600-900 K) thermoelectric materials, specifically PbTe, which has been proven to possess a high energy conversion efficiency of ~ 1.4 as defined by the thermoelectric figure of merit, $zT = S^2T\sigma/(\kappa_E+\kappa_L)$, where S is the Seebeck coefficient, σ is the electrical conductivity, T is the absolute temperature, and κ_L and κ_E are the lattice and electronic thermal conductivity, respectively. However, Te is rare in the Earth's crust, in demand for other applications, and therefore entails high material costs for scale-up. The focus of recent research is to offer inexpensive alternatives by replacing Te with Se or S to form binary PbSe [9-11] or PbS [12, 13] or ternary systems of PbTe-PbSe [4, 14, 15], PbTe-PbS [13, 16-18] and PbSe-PbS [19]. Nevertheless, it is still a big challenge to find a tellurium-reduced Pb-chalcogenide compound that can provide a high *zT* over a wide temperature range.

In a recent report,[20] we demonstrated enhanced thermoelectric performance of single-phase quaternary $(PbTe)_{(1-x-y)}(PbSe)_y(PbS)_x$ alloys compared to binary PbTe, PbSe, PbS, and ternary $(PbTe)_{(1-x)}(PbSe)_x$, $(PbTe)_{(1-x)}(PbS)_x$ systems. The electronic band structure is tuned by soluble PbS, the solubility limit of which is increased in the PbTe matrix in the presence of PbSe. The lattice thermal conductivity is also reduced by phonon scattering on high contrast atomic mass solute atoms. The more extensive report [21] on a similar system $(PbTe)_{(1-2x)}(PbSe)_x(PbS)_x$, confirmed our findings for single phase *p*-type quaternary lead chalcogenides and showed a figure of merit ~ 2 for a single phase alloy with optimised composition and carrier concentrations.

Recent studies [13, 16, 18] have also shown that nanostructuring in the ternary PbTe-PbS system by introducing secondary phases in the matrix, is a viable approach to enhance the thermoelectric efficiency. In the present work, we have fabricated bulk quaternary Pb-chalcogenide nanocomposites through PbS alloying beyond its solubility limit in the $(PbTe)_{0.9}(PbSe)_{0.1}$ matrix. The composition range of the quaternary $(PbTe)_{(1-x-y)}(PbSe)_y(PbS)_x$ system is large and the choice of optimum dopant concentration will add to this complication. Here, the initial investigation on the thermoelectric performance of quaternary lead chalcogenide composites was limited to 1 at% dopant concentration (Na) which corresponds

to $Pb_{0.98}Na_{0.02}Te_{(1-x-y)}Se_yS_x$ in the equivalent formula, and the PbSe concentration was restricted to 10 at% (y = 0.1) in the $(PbTe)_{(1-x-y)}(PbSe)_y(PbS)_x$ system for all samples, to eliminate variations in the electronic band structure of PbTe which can be made by selenium solute atoms similar to the ternary $(PbTe)_{(1-x)}(PbSe)_x$ system [4, 22]. The thermoelectric performance of composite samples are compared to the parent solid solution ternary compound of $(PbTe)_{0.9}(PbSe)_{0.1}$. The electronic band structure alteration is only associated with the fraction of PbS in the $(PbTe)_{(0.9-x)}(PbSe)_{0.1}(PbS)_x$ system.

We provide insight into the fundamental issues regarding the electronic transport properties of nanostructured composite materials with varying secondary phase solubility as a function of temperature. The increased concentration of sulphur in the matrix at high temperatures and variation in secondary phase fraction affects the electronic transport properties of composites.

2. Experimental

2.1. Sample fabrication

Synthesis: Polycrystalline samples of PbS, PbSe, and PbTe were prepared by mixing high purity Pb (99.999%), Te (99.999%), Se (99.999%), and dried S (99.9%) in vacuum sealed quartz ampoules at a residual pressure of ~ 10^{-4} Torr. These were reacted at high temperature to produce high purity PbSe and PbS starting materials. The final polycrystalline $(PbTe)_{(0.9-x)}(PbSe)_{0.1}(PbS)_x$ (x = 0, 0.05, 0.1, 0.15, 0.2, 0.25) samples were synthesized by mixing stoichiometric quantities of high purity PbS, PbSe, Pb, and Te, with 1 mol% Na added as the dopant. A total mass of 10 g was sealed in carbon-coated quartz tubes under vacuum, and then heated to 1373 K with a heating rate of 100 K per hour. After being held at 1373 K for 10 hours, the samples were quenched in cold water, followed by annealing at 773 K for 48 hours.

Sintering: The resulting ingots from the synthesis procedure were hand-ground to powder with a mortar and pestle. They were sintered at 773 K for 1 hour in a 12 mm diameter graphite mould, at an axial pressure of 40 MPa, that was achieved by induction hot pressing under an argon atmosphere [23].

2.2. Transport properties measurements

Resistivity and Hall measurements: Samples were loaded onto a heated BN substrate and four probes were attached to the edge of the sample. The sample was placed in vacuum with a magnetic field (up to ± 2 T) perpendicular to its surface. The resistivity (ρ) and Hall coefficient (R_H) (along the hot-pressing direction) were measured using the van de Pauw method [24].

Seebeck coefficient measurements: The Seebeck coefficients were obtained along the sample's hot pressing direction. The samples were placed in contact with a heater on each surface in a vacuum chamber [25]. Two Nb-Chromel thermocouples were also pressed against the two surfaces of the sample by spring force. The heaters were programmed to provide a temperature difference oscillation of ± 7° C, whilst maintaining a set average temperature. The thermoelectric voltage and temperature on each surface were recorded, with the slope giving the Seebeck coefficient at the average temperature.

Thermal conductivity measurements: The thermal conductivity (κ) was calculated from $\kappa = \rho D_T C_p$. The laser flash method (Netzsch LFA457) was used to measure the thermal diffusivity (D_T), the density (ρ) was calculated using the measured weight and dimensions. The specific heat capacity (C_p), was estimated by $\{Cp(k_B \text{ per atom}) = 3.07 + 4.7 \times 10^{-4} \times (T/K - 300)\}$ [26, 27] that is believed to be accurate for lead chalcogenides [4, 10]. The combined uncertainty for all measurements involved in zT determination is ~ 20%.

2.3. Materials characterisation

X-Ray Diffraction: The crystallographic structure and composition were characterized by X-ray diffraction (XRD) using a PANalytical X'Pert Pro X-Ray diffractometer with Cu K_α radiation (λ = 1.544 Å, 40 kV, 30 mA). In order to measure the phase ratio and to calculate the lattice parameters, the X-ray diffraction patterns were refined using Rietveld analysis.

Electron Microscopy Analyses: Scanning electron microscopy was performed on finely polished samples using a JEOL JSM-7500FA field emission gun-scanning electron microscope (FEG-SEM). Samples were also characterized using a JEOL 2010 transmission electron microscope (TEM). TEM samples were prepared by cutting them into 3 mm diameter discs using a Leica TXP polisher, then grinding and polishing them to less than 100 μm in thickness. The samples were then dimpled, and finally Ar-ion milled on a stage cooled with liquid nitrogen. During ion milling low voltages and currents were used to reduce damage to the samples.

3. Results and discussion

Samples with the composition $(PbTe)_{(0.9-x)}(PbSe)_{0.1}(PbS)_{x,}$ (x = 0, 0.05, 0.1, 0.15, 0.2, 0.25) doped with 1 at% Na on Pb sites, which correspond to an equivalent formula of $Pb_{0.98}Na_{0.02}Te_{(0.9-x)}Se_{0.1}S_x$, were synthesized in ingots by melting and annealing, followed by hot pressing of the hand-ground powders. The selected compositions are located at the PbTe-rich side of the PbTe-PbS system [28], where the phase separation of NaCl-structured PbTe-

rich and PbS-rich phases occurs through the nucleation and growth process. The relevant phase diagram is discussed in details in the Supporting Information.

The purity and crystal structure of the samples were determined by indexing the powder X-ray diffraction (XRD) patterns in **Figure 1**. The XRD patterns of samples with $x < 0.1$ appear to be single phase, whereas samples with $x > 0.1$ reveal two distinct phases. The **Figure 1** inset shows that high angle diffraction peaks are shifted with increasing PbS concentration to 10 at% due to the alloying effect. However, additions above 10 at% produced no further shift. Rietveld refinement was employed to determine the lattice parameters of the matrix accurately by extrapolating from high angle diffraction peaks. The lattice parameters of the matrix and precipitates, and the proportions of secondary phase are summarized in Table 1. The lattice parameter of the secondary phase is larger than for pure PbS (a = 5.93 Å), which indicates that the PbS-rich secondary phase is alloyed with PbSe (a = 6.13 Å) and PbTe (a = 6.46 Å), both of which phases possess larger lattice parameters. The lattice parameter of the matrix varies with PbS addition up to $x = 0.1$, but remains almost constant for $x > 0.1$, as shown in Table 1. This indicates that for samples with $x > 0.1$, the chemical compositions of the matrix and the second phase are fixed at any given temperature, although the weight fraction of the second phase does increase with x above this threshold.

The scanning electron microscope (SEM) image of the sintered sample S15 presented in **Figure 2(a)** illustrates the morphology and wide size distribution of micrometer-sized precipitates in the matrix. The precipitation in multi-grain solids occurs preferentially at grain boundaries due to lower chemical driving force for nucleation and higher diffusion coefficient of elements at grain boundaries than the grains. The segregation of solute atoms to grain boundaries may also occurd during solidification [29]. Therefore, the precipitates at grain boundaries are generally larger than those formed within the crystal. This sample was exposed to several heating/cooling cycles during measurement of transport properties and dissolution and coarsening of precipitates may have occurred. The corresponding transmission electron microscope (TEM) micrograph of the same sample in **Figure 2(b)** shows an extensive population of submicron precipitates throughout the matrix is also present. The morphology of the precipitates is similar to the PbTe-PbS system [30]. Based on the information obtained from the pseudo binary phase diagram of PbTe-PbS [31], the secondary phases are believed to be PbSe alloyed PbS. Precipitates within the lead telluride-rich matrix **(Figure 2(b))** were characterised using electron diffraction. **Figures 2(c)** demonstrates the diffraction pattern from [110] zone axis of the area circled in **Figure 2(b),** selected by an aperture which included matrix and a single precipitate. The precipitate has the

same crystal structure and orientation as the matrix but its lattice parameter is smaller. The large number of additional reflections in the [110] pattern (**Figure 2(c)**) arises from double diffraction. Typically, single scattering of the primary electron beam occurs. However, scattered beams can undergo further scattering giving rises to multiplicity of the original diffraction pattern, offset by the original diffraction vector. **Figure 2(b)** illustrates the bright field image from which the [110] diffraction pattern (**Figure 2(c)**) was obtained. The precipitates show very strong moire fringes, caused by interference between beams scattered from the matrix and precipitate. All precipitates within a single grain exhibit the same contrast/fringe orientation indicating they all have the same orientation with respect to the matrix. More details of the TEM analyses are given in the Supporting Information.

Figure 2(d) shows energy dispersive x-ray spectroscopy (EDS) spectra obtained from the matrix and the precipitate measured from adjacent regions of similar thickness. EDS microanalaysis of the sulphur-rich precipitates is complicated by the fact that the solitary sulphur K_α emission line (2.307keV) overlaps with that of the Pb M_α line (2.342keV). Therefore, the intensity of the precipitate spectrum was normalised to that of the matrix spectrum at the Pb L_α line at 10.56keV. It is clear that the precipitates are compositionally distinct from the matrix with no tellurium spectrum detected. The intensity of the overlapped Pb M_α and S K_α peaks at 2.3keV is marginally greater for the precipitate compared with the matrix. Although precipitates generate sulphur x-rays, the very high mean atomic number of the precipitate would result in strong absorption for such a low energy x-ray. The mass balance and electron diffraction analyses confirm sulphur-rich precipitates.

Table 2 presents the room temperature Hall carrier concentraion ($n_H = r_H /e.R_H$) for composite samples. The hole carrier concentration for all samples is ~ 8×10^{19} cm^{-3}. The sodium concentration was restricted to 1 at% in the current study due to low reported maximum solubility of sodium in PbTe[32, 33]. However, the room temperature hole carrier concentration for samples in Table 2 is ~ 8×10^{19} cm^{-3} that is lower than the optimum carrier concentrations for *p*-type Pb-chalcogenides.[4, 6, 10, 16, 34] The samples are highly degenerate semiconductors, while enhanced thermoelectric efficiency is anticipated for the current study compounds at optimum hole carrier concentrations.

The electrical resistivity, Seebeck coefficient, measured total thermal conductivity, κ, and calculated lattice thermal conductivity, κ_L, for sodium-doped $(PbTe)_{(0.9-x)}(PbSe)_{0.1}(PbS)_x$, ($x$ =0, 0.05, 0.1, 0.15, 0.2, and 0.25) composite samples as a function of temperature in the range of 300-850 K are compared with single phase sodium doped $(PbTe)_{(0.9-}$

$_{x)}(PbSe)_{0.1}(PbS)_{x,}$ (x = 0 and 0.05) samples [20] in **Figure 3**. All samples show the typical behaviour of strongly degenerate semiconductors, with the Seebeck coefficient and electrical resistivity increasing with temperature. It should be noted that the resistivity curves for all samples containing the PbS-rich secondary phase, show different behaviour on heating and cooling over a temperature range of approximately 500-700 K. The selected heating and cooling rates are 100 ˚C/h. **Figure 3(a)** shows the smooth decrease in resistivity as a function of temperature for Na-doped $(PbTe)_{(0.9-x)}(PbSe)_{0.1}(PbS)_{x,}$ (x = 0.1, 0.15, 0.2, and 0.25) samples upon cooling from 850K. The resistivity curves of single phase samlples, (x = 0 and 0.05) indicate the same trend during cooling and heating.[20] The resistivity of composite samples, $(PbTe)_{(0.9-x)}(PbSe)_{0.1}(PbS)_{x,}$ (x = 0.1, 0.15, 0.2, and 0.25), during heating in **Figure 3(d)** show relatively distinct behaviour for samples with a distinct secondary phase fraction. The cycle was repeated several times, and various heating rates were employed to confirm the presence of hysteresis in the resistivity for the composite samples. Although the peak temperature and the slope of the curve vary slightly with the heating rate, the cooling curve trends were independent of the rate. This behaviour might be attributed to the sodium partitioning [30, 32], and the changes in the distribution and morphology of secondary phases [35]. This is discussed in more details elsewhere.[36]

Figure 3(a) shows that the electrical resistivity is increased considerably by sulphide addition up to the solubility limit (x < 0.1). However, sulphide additions above this level, which increases the precipitate fraction, cause only minor further increase in electrical resistivity. The electrical resistivity of single phase alloys is increased by sulphide addition due to the scattering of carriers from disordered atoms [37], and possibly due to the increase in the effective mass of the light-band by alloying with sulphur.

In our recent report [20], we indicated that the addition of PbS to sodium-doped solid solution PbSe-PbTe up to the solubility limit provides a considerably lower thermal conductivity, a heavier density of states effective mass, a wider band gap, and a larger energy offset between valence bands. This results in a higher temperature for band convergence and a larger Seebeck coefficient in sulphur-containing samples and provides a thermoelectric efficiency superior to binary PbQ (Q= Te, Se, S) and ternary systems of PbTe-PbSe and PbTe-PbS. These results have been confirmed by a more recent report on single phase *p*-type quaternary $(PbTe)_{(1-2x)}(PbSe)_x(PbS)_x$ alloys [21]. The chemical compositions of the matrix and the second phase are fixed at any given temperature for nanocomposite samples (x > 0.1) and the weight fraction of the secondary phase increases with *x;* while, as the temperature increases, the solubility limit of PbS-rich precipitates increases in the matrix of composite samples, and

the chemistry of material is changed. The nanostructuring through transformation [17, 38, 39] and/or precipitation [13, 16], generally involves a significant fraction of secondary phases. The physical properties of a composite material are related to the volume fraction and the physical properties of the individual components of the composite. and various equations have been developed to model these associations [40, 41]. It is beyond the scope of the current study to quantitatively describe the contribution of secondary phases on electronic transport properties of the current study composites, suffice it to state that the chemical composition deviation at high temperatures along with variation of secondary phase fractions results in unpredicted behaviour of resistivity and Seebeck coefficient of composite samples with a large fraction of secondary phases (x = 0.15, 0.20 and 0.25).

The thermal conductivities of single phase quaternary Pb chalcogenides which are alloyed marginally with PbS (up to 10 at%) are considerably lower than parent compounds of $(PbTe)_{(1-x)}(PbSe)_x$[20, 21]. Surprisingly, the room temperature thermal conductivity of nanostructured samples, which contains secondary sulphide phase (**Figure 3(c)**), is only slightly lower than the thermal conductivity of a single phase alloy of $(PbTe)_{0.85}(PbSe)_{0.1}(PbS)_{0.05}$ which contains 5 at% soluble PbS. This difference is negligible at higher temperatures. The lower thermal conductivities of the phases containing secondary sulphide, compared to PbS-free single phase alloys might be attributed to phonon scattering on solute atoms with large mass contrast [42] and/or phonon scattering at defects and interfaces originated from the distributed sulphide secondary phase[16]. In order to fully realize this effect, the lattice thermal conductivity, κ_L, was obtained by subtracting the electronic component, κ_e. The value of the charge carrier thermal conductivity κ_e can be determined via the Wiedemann-Franz relation, $\kappa_e = LT/\rho$, where ρ is the resistivity, and L is the Lorenz number estimated as a function of temperature, assuming a parabolic band with acoustic phonon scattering.[43] This rough estimation has been shown to be reasonably consistent with a more detailed model calculation taking the band parabolicity and multiband conduction effects into account [4]. (See supporting information).

A low room-temperature lattice thermal conductivity of ~1.2 W/m·K is observed for the sample with x = 0.15, which is reduced to ~0.6 W/m·K at temperatures above 650 K, whereas the lattice thermal conductivity is increased for Samples with x = 0.2 and 0.25. **Table 3** summarizes the total and lattice thermal conductivities of Na-doped $(PbTe)_{(0.9-x)}(PbSe)_{0.1}(PbS)_x$, ($x$ = 0, 0.05, 0.1, 0.15, 0.2, and 0.25) samples at room temperature and 850 K. The phonon scattering on solute atoms with large mass contrast [42] and on interfaces of

nanoprecipitates [16] reduces the lattice thermal conductivity of alloys containing sulphur up to $x = 0.15$. However, further addition of sulphides to the quaternary system results in a larger secondary phase volume fraction in the composite. The lattice thermal conductivity of PbS is higher than that of PbTe [44], and a large volume fraction of PbS precipitates in samples with $x > 0.2$ results in a subsequent increase in their lattice thermal conductivity.

Figure 4(a) compares measured zT up to 850 K for composite samples of $(PbTe)_{(0.9-x)}(PbSe)_{0.1}(PbS)_{x,}$ ($x = 0.1$, 0.15, 0.2, and 0.25) to single phase alloys with $x = 0$ and 0.05 [20]. The maximum zT value of 1.6 was achieved at 750 K for the single-phase sample with $x = 0.05$ while the thermoelectric efficiency is reduced for composite compounds. Although a high thermoelectric efficiency of ~1.4 has been achieved for the composite sample with $x = 0.25$, the figure of merit of composite compounds and alloys with a secondary phase, are lower than single phase alloys. This efficiency is obtained in the sample, where 35% of tellurium atom sites are occupied by the abundant elements selenium and sulphur.

The thermoelectric figure of merit of the *p*-type composite $(PbTe)_{0.65}(PbSe)_{0.1}(PbS)_{0.25}$ in the current study is compared with the maximum zT values reported for *p*-type tellurium-free PbSe [10], strontium-added PbS [12], CdS-added PbSe [45], single phase PbTe [34], tellurium-reduced PbTe-12 at% PbS [16], and PbTe-16 at% PbS [16] composites with identical dopant concentration in **Figure 4(b)**. A figure of merit of over 1 has been obtained at temperatures above 600 K, compared with 750 K for *p*-type PbSe [10] and 800 K for *p*-type strontium-added PbS [12]. The high zT obtained at lower temperatures can enhance the power generation efficiency of thermoelectric devices. The nano-composite sample containing only 32.5 at% Tellurium, $(PbTe)_{0.65}(PbSe)_{0.1}(PbS)_{0.25}$, shows similar efficiency to PbTe [34] and $(PbTe)_{0.88}(PbS)_{0.12}$ [16] with much higher tellurium content, while it has considerably higher thermoelectric efficiency than PbSe [10, 45], strontium-added PbS [12] and $(PbTe)_{0.84}(PbS)_{0.16}$ [16] with lower tellurium content.

4. Conclusion

In summary, we demonstrate high thermoelectric efficiency in *p*-type composite quaternary Pb-chalcogenides where tellurium is replaced by the abundant elements selenium and sulphur. The partial dissolution of sulphide precipitates in the matrix at elevated temperatures results in a higher Seebeck coefficient than in single phase alloys in combination with reasonably low electrical resistivity. Our results show that the very low achieved thermal conductivity is dominated by phonon scattering at high contrast atomic mass solute atoms rather than at distributed secondary phases within the matrix. We show that the thermal

conductivity of composites with a considerable fraction of sulphide precipitates is higher than for single phase sulphur-alloyed compounds, but still lower than for the sulphur-free compound. Our results are a step forward in realising the thermoelectric performance of multiphase alloys in quaternary Pb chalcogenides with lower tellurium concentration.

Acknowledgements

This work is supported by Australian Research Council (ARC) Discovery Early Career Award DE130100310, the Department of Education, Science and Technology (DEST) of Australia, the Materials Project funded by U.S. Department of Energy's Basic Energy Sciences program under Grant No. EDCBEE, DOE contract DE-AC02-05CH11231 and the Air Force Office of Scientific Research – Multidisciplinary Research Program of the University Research Initiative (AFOSR-MURI) and the Russian Ministry of Education.

Reference

[1] Bell LE. Science 2008;321:1457.
[2] Shi X, Yang J, Bai S, Yang J, Wang H, Chi M, Salvador JR, Zhang W, Chen L, Wong-Ng W. Adv. Funct. Mater. 2010;20:755.
[3] Shi X, Yang J, Salvador JR, Chi M, Cho JY, Wang H, Bai S, Yang J, Zhang W, Chen L. J. Am. Chem. Soc. 2011;133:7837.
[4] Pei Y, Shi X, LaLonde A, Wang H, Chen L, Snyder GJ. Nature 2011;473:66.
[5] Heremans JP, Jovovic V, Toberer ES, Saramat A, Kurosaki K, Charoenphakdee A, Yamanaka S, Snyder GJ. Science 2008;321:554.
[6] Biswas K, He J, Zhang Q, Wang G, Uher C, Dravid VP, Kanatzidis MG. Nature Chem. 2011;3:160.
[7] Božin ES, Malliakas CD, Souvatzis P, Proffen T, Spaldin NA, Kanatzidis MG, Billinge SJL. Science 2010;330:1660.
[8] Biswas K, He J, Blum ID, Wu C-I, Hogan TP, Seidman DN, Dravid VP, Kanatzidis MG. Nature 2012;489:414.
[9] Androulakis J, Lee Y, Todorov I, Chung D-Y, Kanatzidis M. Phys. Rev. B 2011;83:195209.
[10] Wang H, Pei Y, LaLonde AD, Snyder GJ. Adv. Mater. 2011;23:1366.
[11] Wang H, Pei Y, Lalonde AD, Snyder GJ. Proc. Natl. Acad. Sci. U.S.A. 2012;109:9705.
[12] Zhao L-D, He J, Wu C-I, Hogan TP, Zhou X, Uher C, Dravid VP, Kanatzidis MG. J. Am. Chem. Soc. 2012;134:7902.
[13] Johnsen S, He J, Androulakis J, Dravid VP, Todorov I, Chung DY, Kanatzidis MG. J Am. Chem. Soc. 2011;133:3460.
[14] Zhang Q, Cao F, Liu W, Lukas K, Yu B, Chen S, Opeil C, Broido D, Chen G, Ren Z. J Am. Chem. Soc. 2012;134:10031.
[15] Kudman I. Journal of Materials Science 1972;7:1027.
[16] Girard SN, He J, Zhou X, Shoemaker DP, Jaworski CM, Uher C, Dravid VP, Heremans JP, Kanatzidis MG. J. Am. Chem. Soc. 2011;133:16588.

[17] Girard SN, He J, Li C, Moses S, Wang G, Uher C, Dravid VP, Kanatzidis MG. Nano Lett. 2010;10:2825.
[18] He J, Girard SN, Kanatzidis MG, Dravid VP. Adv. Funct. Mater. 2010;20:764.
[19] Androulakis J, Todorov I, He J, Chung D-Y, Dravid V, Kanatzidis M. J. Am. Chem. Soc. 2011;133:10920.
[20] Aminorroaya Yamini S, Wang H, Gibbs Z, Pei Y, Dou SX, Snyder GJ. Phys. Chem. Chem. Phys. 2014;16:1835.
[21] Korkosz RJ, Chasapis TC, Lo S-h, Doak JW, Kim YJ, Wu C-I, Hatzikraniotis E, Hogan TP, Seidman DN, Wolverton C, Dravid VP, Kanatzidis MG. J Am. Chem. Soc. 2014.
[22] Jaworski CM, Wiendlocha B, Jovovic V, Heremans JP. Energy Environ. Sci. 2011;4:4155.
[23] LaLonde AD, Ikeda T, Snyder GJ. Rev. Sci. Instrum. 2011;82:025104.
[24] Borup KA, Toberer ES, Zoltan LD, Nakatsukasa G, Errico M, Fleurial J-P, Iversen BB, Snyder GJ. Rev. Sci. Instrum. 2012;83:123902.
[25] Iwanaga S, Toberer ES, LaLonde A, Snyder GJ. Rev. Sci. Instrum. 2011;82:063905.
[26] Blachnik R, Igel R. Z. Naturforsch. B 1974;29:625.
[27] Pashinkin AS, Mikhailova MS, Malkova AS, Fedorov VA. Inorg. Mater. 2009;45:1226.
[28] Volykhov A, Yashina L, Shtanov V. Inorg. Mater. 2006;42:596.
[29] Priester L. Precipitation at grain boundaries. In: Grain boundaries: From theory to Engineering, vol. 172. Springer, Heidelberg, 2013.
[30] He J, Blum ID, Wang H-Q, Girard SN, Doak J, Zhao L-D, Zheng J-C, Casillas G, Wolverton C, Jose-Yacaman M, Seidman DN, Kanatzidis MG, Dravid VP. Nano Lett. 2012;12:5979.
[31] Volykhov A, Yashina L, Shtanov V. Inorg. Mater. 2010;46:464.
[32] He J, Zhao L-D, Zheng J-C, Doak JW, Wu H, Wang H-Q, Lee Y, Wolverton C, Kanatzidis MG, Dravid VP. J. Am. Chem. Soc. 2013;135:4624.
[33] Aminorroaya Yamini S, Ikeda T, Lalonde A, Pei Y, Dou SX, Snyder GJ. J. Mater. Chem. A 2013;1:8725.
[34] Pei Y, LaLonde A, Iwanaga S, Snyder GJ. Energy Environ. Sci. 2011;4:2085.
[35] Gelbstein Y. Acta Mater. 2013;61:1499.
[36] Aminorroaya Yamini S, Wang H, Gibbs Z, Pei Y, David Mitchel, Dou SX, Snyder GJ. Unpublished manuscript 2014.
[37] Wang H, LaLonde AD, Pei Y, Snyder GJ. Adv. Funct. Mater. 2012;23:1586.
[38] Gelbstein Y, Davidow J, Girard SN, Chung DY, Kanatzidis M. Adv. Energy Mater. 2013;3:815.
[39] Androulakis J, Lin C-H, Kong H-J, Uher C, Wu C-I, Hogan T, Cook BA, Caillat T, Paraskevopoulos KM, Kanatzidis MG. J. Am. Chem. Soc. 2007;129:9780.
[40] Ashby MF, Bréchet YJM. Acta Mater. 2003;51:5801.
[41] Gorsse S, Bellanger P, Brechet Y, Sellier E, Umarji A, Ail U, Decourt R. Acta Mater. 2011;59:7425.
[42] Wang H, Schechtel E, Pei Y, Snyder GJ. Adv. Energy Mater. 2012;3:488.
[43] May AF, Toberer ES, Saramat A, Snyder GJ. Phys. Rev. B 2009;80:125205.
[44] Ravich YI, Efimova BA, Smirnov IA. Semiconducting lead chalcogenides Plenum Press in New York, 1970.
[45] Zhao L-D, Hao S, Lo S-H, Wu C-I, Zhou X, Lee Y, Li H, Biswas K, Hogan TP, Uher C, Wolverton C, Dravid VP, Kanatzidis MG. J Am. Chem. Soc. 2013;135:7364.

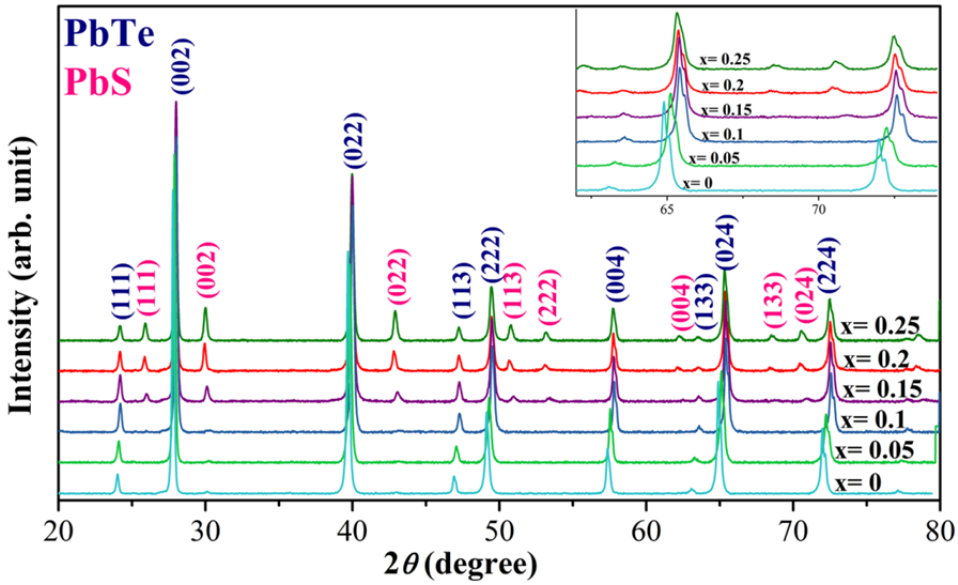

Figure 1. Room temperature X-ray diffraction patterns for $(PbTe)_{(0.9-x)}(PbSe)_{0.1}(PbS)_x$ (x = 0, 0.05, 0.1, 0.15, 0.2 and 0.25) alloys. The inset shows shifting of diffraction peaks to higher angles for x up to 0.1 due to the alloying effect.

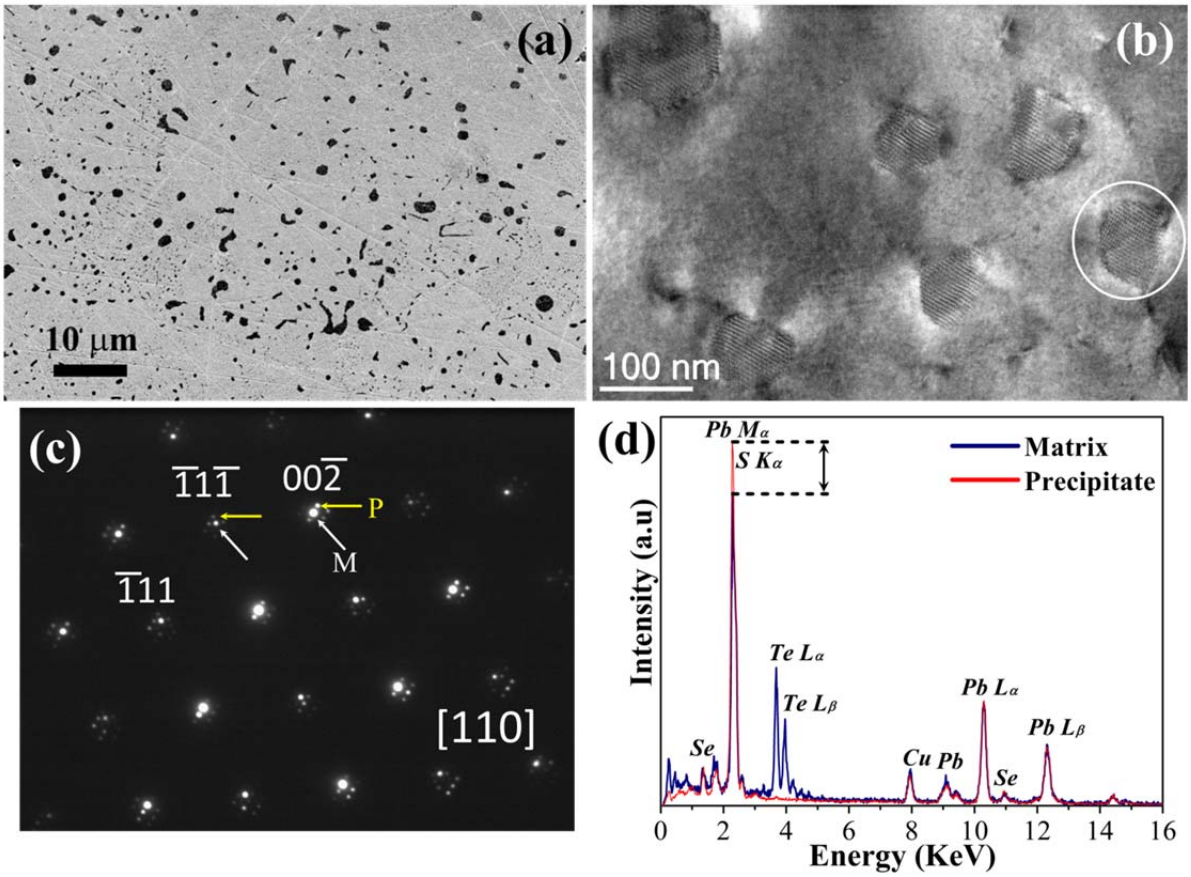

Figure 2. (a) SEM image of sintered $(PbTe)_{0.75}(PbSe)_{0.1}(PbS)_{0.15}$ (S15) sample, showing the morphology and the distribution of precipitates in the matrix, the sample has been through several cycles of heating up to 850 K and cooling during transport properties measurements; **(b)** Bright field TEM micrograph of sulphur-rich precipitates in the tellurium-rich matrix

when the matrix was titled to [110] zone axis in the $(PbTe)_{0.75}(PbSe)_{0.1}(PbS)_{0.15}$ (S15) sample shown in (a). Strong moire patterns are observed due to the double diffraction; **(c)** The experimental selected area diffraction pattern (SADP) obtained from the precipitate ringed in (b), The diffraction spots are marked for precipitates and matrix by P and M respectively; **(d)** EDS spectra obtained from the matrix and precipitate. Precipitate intensities have been normalised to match matrix intensities at the Pb L_α line at 10.55keV. The precipitate contains no Te and is clearly a distinct phase. The Pb M_α and S K_α lines overlap at 2.3keV and this peak is marginally more intense for the precipitate (Pb + S) compared with the matrix (Pb only).

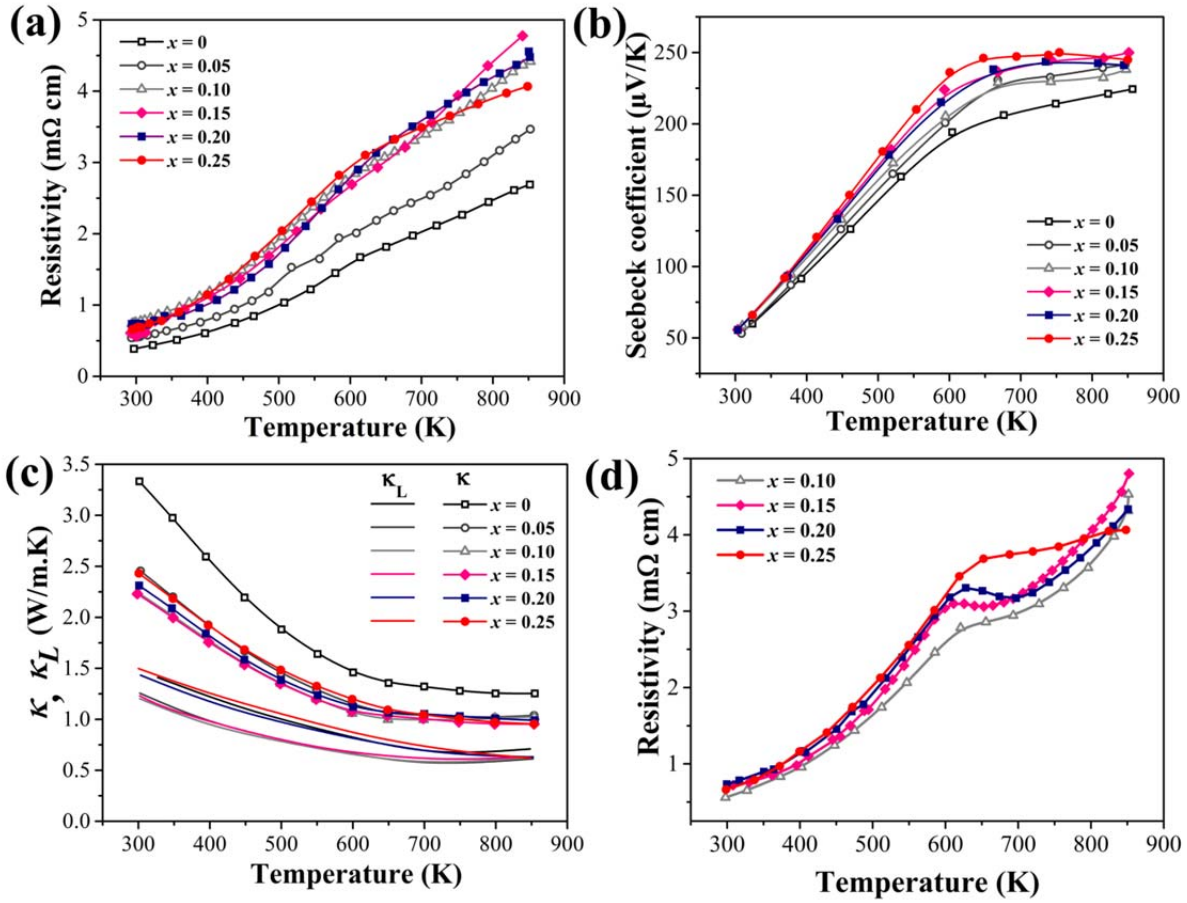

Figure 3. Thermoelectric transport properties of $(PbTe)_{(0.9-x)}(PbSe)_{0.1}(PbS)_x$, (x = 0, 0.05, 0.1, 0.15, 0.2, 0.25) sintered bulk samples doped with 1 at% Na: (a) electrical resistivity (mΩ·cm), cooling curves; (b) Seebeck coefficient (μV/K) temperature dependence; (c) measured total thermal conductivity, κ (W/m·K), and calculated lattice thermal conductivity κ_L, with the Lorenz factor approximated using a single parabolic band model with acoustic scattering; (d) electrical resistivity (mΩ·cm) of Na-doped $(PbTe)_{(0.9-x)}(PbSe)_{0.1}(PbS)_x$, ($x$ = 0.1, 0.15, 0.2, and 0.25) sintered bulk sample during heating.

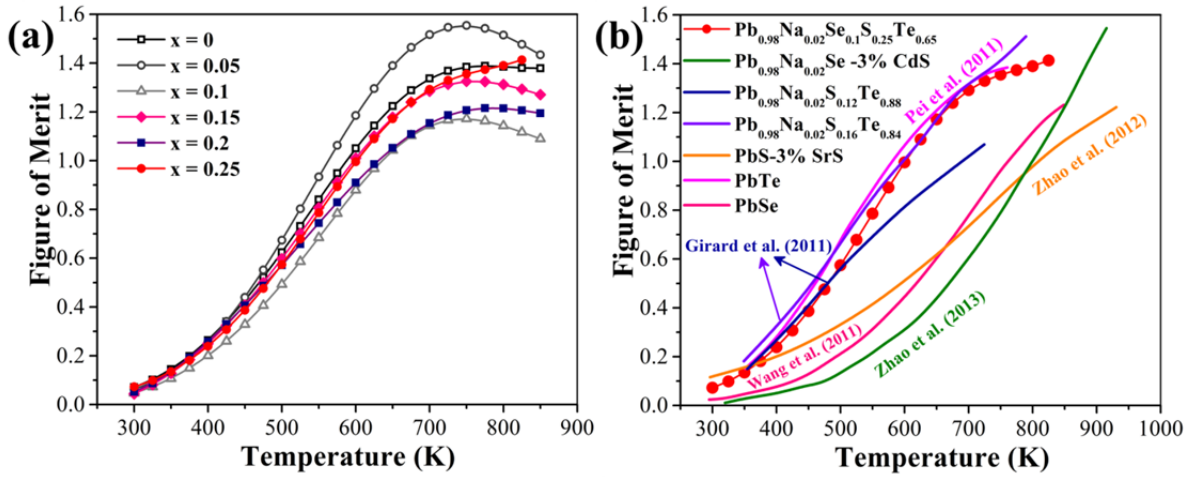

Figure 4. (a) Temperature dependence of the dimensionless figure of merit *zT* for 1 mol% Na-doped $(PbTe)_{(0.9-x)}(PbSe)_{0.1}(PbS)_x$, (x = 0, 0.05, 0.1, 0.15, 0.2, 0.25) sintered bulk samples; (b) comparison of the thermoelectric efficiency of the nanocomposite $Pb_{0.98}Na_{0.02}S_{0.25}Se_{0.1}Te_{0.65}$ quaternary system with maximum reported values for binary *p*-type PbSe[10], *p*-type strontium-added PbS,[12] *p*-type CdS-added PbSe,[45] and *p*-type PbTe,[34] PbTe-12 at% PbS,[16] and PbTe-16 at% PbS,[16] indicating larger efficiency over a wide temperature range.

Table 1. Lattice parameters and percentage of precipitates in the matrix.

Sample number	Lattice parameter of matrix PbTe(Se) (Å)	Lattice parameter of PbS(Se), precipitates (Å)	Weight percentage of precipitates
$x = 0$	6.423	-	-
$x = 0.05$	6.406	-	-
$x = 0.1$	6.379	-	-
$x = 0.15$	6.381	5.945	4.7±0.2
$x = 0.20$	6.384	5.968	11.1±0.3
$x = 0.25$	6.389	5.975	16.8±0.4

Table 2. The Hall carrier concentration of Na-doped $(PbTe)_{(0.9-x)}(PbSe)_{0.1}(PbS)_x$ (x = 0.1, 0.15, 0.2, and 0.25) composite samples at room temperature.

Sample number	Carrier concentration (cm^{-3})
x= 0.10	8.3×10^{19}
x= 0.15	8.1×10^{19}
x= 0.20	7.3×10^{19}
x= 0.25	7.8×10^{19}

Table 3. The total and lattice thermal conductivity of $(PbTe)_{(0.9-x)}(PbSe)_{0.1}(PbS)_x$, (x = 0, 0.05, 0.1, 0.15, 0.2, 0.25) sintered bulk samples doped with 1 at% Na at room temperature and 850 K.

Sample	The room temperature lattice thermal conductivity	The room temperature total thermal conductivity	The lattice thermal conductivity at 850 K
$x = 0$	1.4	3.3	0.7
$x = 0.05$	1.26	2.5	0.6
$x = 0.10$	1.2	2.3	0.6
$x = 0.15$	1.2	2.2	0.6
$x = 0.20$	1.4	2.3	0.6
$x = 0.25$	1.5	2.4	0.6